

Piezoresistive behavior of amorphous carbon films for high performance MEMS force sensors

Cite as: Appl. Phys. Lett. **114**, 253502 (2019); <https://doi.org/10.1063/1.5096225>

Submitted: 15 March 2019 . Accepted: 08 June 2019 . Published Online: 24 June 2019

Xin Ma , Peng Guo, Xiaoshan Tong , Yulong Zhao , Qi Zhang, Peiling Ke, and Aiyong Wang 



View Online



Export Citation



CrossMark

Lock-in Amplifiers up to 600 MHz

starting at

\$6,210



 Zurich Instruments

Watch the Video 

Piezoresistive behavior of amorphous carbon films for high performance MEMS force sensors

Cite as: Appl. Phys. Lett. **114**, 253502 (2019); doi: [10.1063/1.5096225](https://doi.org/10.1063/1.5096225)

Submitted: 15 March 2019 · Accepted: 8 June 2019 ·

Published Online: 24 June 2019



View Online



Export Citation



CrossMark

Xin Ma,^{1,2,a)}  Peng Guo,^{2,a)} Xiaoshan Tong,¹  Yulong Zhao,¹  Qi Zhang,^{1,b)} Peiling Ke,^{2,3} and Aiyang Wang^{2,3,b)} 

AFFILIATIONS

¹The State Key Laboratory for Mechanical Manufacturing Systems, Xi'an Jiaotong University, Xi'an 710049, China

²Key Laboratory of Marine Materials and Related Technologies, Zhejiang Key Laboratory of Marine Materials and Protective Technologies, Ningbo Institute of Materials Technology and Engineering, Chinese Academy of Sciences, Ningbo 315201, China

³Center of Materials Science and Optoelectronics Engineering, University of Chinese Academy of Sciences, Beijing 100049, China

^{a)}Contributions: X. Ma and P. Guo contributed equally to this work.

^{b)}Authors to whom correspondence should be addressed: zhq0919@xjtu.edu.cn, Tel.: +86-029-83395334 and aywang@nimte.ac.cn, Tel.: +86-574-86685170.

ABSTRACT

In this study, microelectromechanical systems (MEMS) force sensors based on H-free amorphous carbon (a-C) films with controlled piezoresistive behavior were fabricated by a facile magnetron sputtering technique. By adjusting the substrate bias voltage from 0 V (floating state) to -350 V, the gauge factor (GF) of the a-C film was modulated in the range of 1.4–12.1. Interestingly, the GF showed a strong dependence on the sp^2 content and the sp^2 cluster size of the film, which was consistent with the theory of thick film resistors. In addition, the sensitivity of a-C based MEMS force sensors reached $80.7 \mu V/V/N$ in the force range of 0–1.16 N, with a nonlinearity of approximately 1.3% full scale and good repeatability in over 5000 test cycles.

Published under license by AIP Publishing. <https://doi.org/10.1063/1.5096225>

With the advent of wireless technologies and electrical microelectromechanical systems (MEMS), various functional materials have been developed or fabricated in an attempt to improve the sensitivity, repeatability, and self-adaptability to harsh environments of MEMS piezoresistive sensors. Some examples of these materials are graphene, carbon nanotubes, and silicon nanowires.^{1–3} However, it is important to bear in mind the complex *in situ* growth techniques and fragile transfer of these materials for sensor integration. As such, the current challenges for MEMS force sensors are to enhance production of promising materials with high piezoresistive performance using facile technology.

Amorphous carbon (a-C) and hydrogenated amorphous carbon (a-C:H) films have been proposed as promising piezoresistive thin-film materials for the fabrication of next generation MEMS sensors, because of their low deposition temperature, good uniformity over a large area, excellent mechanical and anticorrosion properties,^{4,5} as well as tunable electrical properties.^{6,7} Recently, high piezoresistive gauge factors (GF) up to 1200 and giant negative GF up to -3200 have been obtained for amorphous carbon films with a different atomic carbon bond structure.^{8–11} Furthermore, the role of H atoms, the sp^3/sp^2 ratio, and the sp^2 cluster size in piezoresistive behavior of a-C/a-C:H films

has also been studied. Tibrewala *et al.* reported that the presence of H atoms in the films could greatly affect their GF. In their study, they reported a GF of approximately 50 and a range of 100–1200 for a-C and a-C:H films, respectively.⁹ The interaction between the conductive sp^2 clusters and the insulative sp^3 matrix was assumed to be the key reason for obtaining different GF values, which was explained by the theory of thick film resistors.^{12–14} Furthermore, Meškinis and co-workers found that the value of the gauge factor (K) in a-C films increased both with the increase in the sp^3/sp^2 ratio and with the decrease in the sp^2 cluster size and that the relationship between K and the resistivity of a-C films (R) followed the $K \sim \log(R)$ law, which was discussed from the perspective of percolating metal and the insulator composite model.¹⁵ On the other hand, different types of a-C based piezoresistive devices were investigated for a wide range of MEMS applications. Peiner *et al.* fabricated a MEMS force test structure to measure the GF of a-C:H films and a microforce sensor, using a-C as a piezoresistor.^{8,13} After transferring the a-C film onto a polyethylene substrate using the lift-off method, Wang *et al.* synthesized a flexible strain sensor with good repeatability even after multiple bending.¹⁶ To date, however, deciphering the piezoresistive mechanism of amorphous carbon films is an ongoing challenge because of the diversity of

amorphous carbon films and their dependence on the deposition process. In addition, more studies are necessary for the use of functionalized a-C films in the production of MEMS force sensors with high piezoresistive performance.

In this study, we selected the H-free a-C film because of the structural simplicity of its amorphous carbon materials and a-C films with various sp^2 contents and sp^2 cluster sizes. These materials were deposited over a large area using a DC magnetron sputtering system. The effect of atomic carbon bonds on the piezoresistive behavior of a-C films was investigated. In addition, a-C based MEMS force sensors were designed and fabricated using MEMS processing. Subsequently, the sensitivity, nonlinearity, and repeatability of the force sensor were evaluated.

The a-C films were deposited by a DC magnetron sputtering technique with a graphite target of 99.9% purity. Various substrate bias voltages of 0 V, -50 V, -100 V, -200 V, -300 V, and -350 V were used to adjust the sp^2 content and the sp^2 cluster size. The base pressure of the vacuum chamber was kept at 2.7×10^{-3} Pa. Four inch SiO_2 /silicon wafers (n-type $\langle 100 \rangle$) were used as substrates. The distance from the substrates to the graphite target was approximately 10 cm. Before deposition, all substrates were etched and pre-cleaned in Ar^+ plasma glow for 30 min, with a substrate bias voltage of -350 V and a work pressure of 1.1 Pa. During film deposition, 65 sccm Ar gas was introduced in the graphite target, with a work pressure of 0.3 Pa and a DC sputtering power of 2.1 kW. The thickness of the a-C films was controlled at approximately 179 ± 6 nm (more details can be found in [supplementary material SI](#)).

Scanning electron microscopy (SEM, Gemini 500, Zeiss) was used to study the morphology of the a-C films. A scratch tester (CSM Revetest scratch tester) was used to test the adhesive force between the film and the substrate. The atomic carbon bonds and chemical composition were evaluated by Raman spectroscopy (InVia-reflex, Renishaw, 532 nm) and X-ray photoelectron spectroscopy (XPS, Axis Ultra DLD). The Gaussian-Lorentzian functions were fitted to the acquired spectra. The GFs of the a-C films were measured using a homemade three-point testing device, which consisted of an analysis balance (XS105 DU, Mettler Toledo) to measure the force applied to the force sensor, a desktop multimeter (Fluke 8846A) to record electric signals, and other auxiliary components. Using MEMS techniques,

a-C force sensors were batch fabricated, and the sensitivity, nonlinearity, and repeatability of the sensors were tested in an atmospheric environment.

Figures 1(a)–1(d) show the large-area fabrication processes of the integrated MEMS force sensor. Four inch silicon substrates (n-type $\langle 100 \rangle$) with dry-oxygen oxidation SiO_2 films on their surfaces were used to obtain high electrical insulation. Since the deposition temperature during the a-C fabrication process was maintained below $40^\circ C$, metals or other heat-resistant masks were not needed, and photoresist could be directly used as a mask for the a-C piezoresistors, as shown in Fig. 1(a). After the a-C films were deposited on the substrates with a designed mask [Fig. 1(b)], a lift-off process was used for structuring a-C piezoresistors, and the photoresist mask was removed by a 10 min acetone ultrasonic process as shown in Fig. 1(c). Next, 20 nm Cr and 200 nm Au films were successively deposited by other magnetron sputtering sources in the chamber to make an electrical connection by using the lift-off process [Fig. 1(d)]. For fabrication of the backside structure, an inductively coupled plasma (ICP) etching process was employed, and the thickness of the silicon diaphragm was kept at approximately $170 \pm 10 \mu m$ ([supplementary material SI](#)). The SEM images depicting the cross section of the a-C piezoresistor and the optical micrograph are shown in Figs. 1(e) and 1(f), where the smooth interface and the intact piezoresistor can be seen. The images of the four inch substrate and the final sensor are shown in Figs. 1(g) and 1(h). In this study, a-C films showed high adhesion to silicon substrates, and the value of L_{c3} (spallation inside the groove)¹⁷ increased to 7.2 N for the -200 V samples and to 8.9 N for the -350 V samples ([supplementary material SI](#)). This was one of the key factors in the fabrication of the a-C piezoresistor.

The Raman spectra of the a-C films are shown in Fig. 2(a). All the Raman spectra showed a typical broadband characteristic of amorphous carbon in the wavelength range of 800 to 2000 cm^{-1} . The curve fitting was carried out by using a Gaussian function to identify the position and area of the D and G peaks. As shown in Fig. 2(b), the fitted I_D/I_G ratio did not show significant changes with a substrate bias voltage in the range of 0 to -200 V. However, it increased substantially to 2.48 when the bias voltage was increased to -300 V, and it then showed a dramatic decline to 2.19 for the substrate bias voltage of -350 V. In general, it is empirically well known that the I_D/I_G ratio

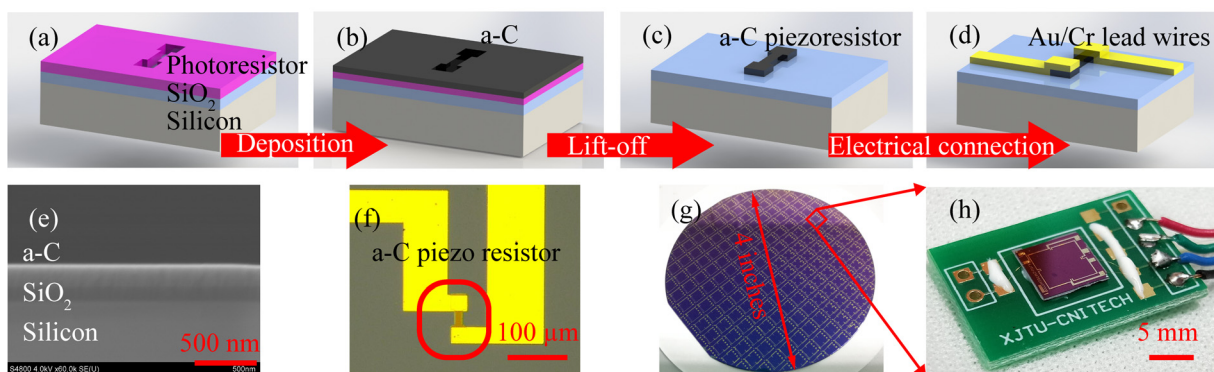


FIG. 1. Schematic of the fabrication process of the a-C diaphragm type force sensor, photolithography (a), a-C deposition (b), lift-off (c) and electrical connection (d), the cross-sectional SEM image of a-C and the substrate (e), the optical microscopy image of the a-C piezoresistor (f), the image of a 4-in. substrate (g), and the packaged force sensor (h) (more details can be found in [supplementary material SI](#)).

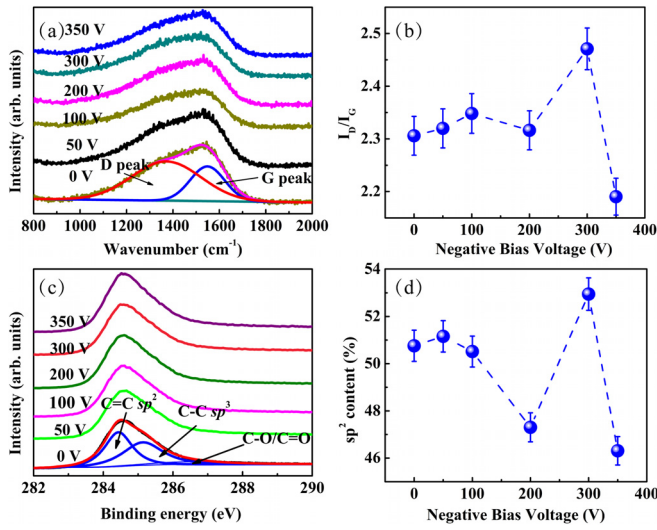


FIG. 2. Raman spectra of the films (a), the correlation between fitted values of I_D/I_G and negative bias voltage (b), XPS C 1s figure of the a-C films (c), and the correlation between the fitted sp^2 content and negative bias voltage (d).

shows a close correlation with the sp^2 cluster size (L_a) in a-C films,¹⁸ where an increase in the I_D/I_G ratio reflects an increase in L_a . In order to evaluate the evolution of the sp^2/sp^3 content in the a-C films with substrate bias control, the XPS C 1s spectra and the fitted result of sp^2/sp^3 in a-C films were studied. These results are illustrated in Figs. 2(c) and 2(d). The 284.6 eV, 285.4 eV, and 286.5 eV binding peaks shown in Fig. 2(c) correspond to the sp^2 hybridization (C=C), sp^3 hybridization (C-C), and C-O/C=O hybridization, respectively.¹⁹ It can be observed that the changes in the sp^2 content showed a similar tendency to that of the I_D/I_G ratio with a change in bias voltage. Specifically, the sp^2 content dropped from 51% to 47.3% as the bias voltage increased from -50 V to -200 V, and it rapidly increased to 52.9% in the case of a bias voltage of -300 V, which was followed by a significant decrease to 46.3% with a bias voltage of -350 V (more details can be found in supplementary material SII). Based on the Raman and XPS results, it could be deduced that adjusting the substrate bias voltage yielded changes in the sp^2 content and the sp^2 cluster size. The minimum sp^2 content and cluster size were obtained at a substrate bias voltage of -350 V in a-C films.

Figures 3(a) and 3(b) show the home-made GF testing device using a three-point method and the measured GFs for a-C films. In this study, K was calculated by²⁰

$$K = \frac{l^2}{3t\Delta Y} \frac{\Delta R}{R_0}, \quad (1)$$

where l is the distance between two support points, t is the thickness of the sample, ΔY is the change in midpoint vertical positioning after loading, ΔR is the change in resistance, and R_0 is the initial resistance.

As shown in Fig. 3(b), the GFs of the a-C films were changed from 1.4 to 12.1 with the substrate bias voltage spanning a range of 0 V to -350 V. In particular, the evolution of GFs showed strong correlation with a change in the sp^2 content and the sp^2 cluster size, L_a , in the a-C films. When the bias voltage was maintained at -350 V, the

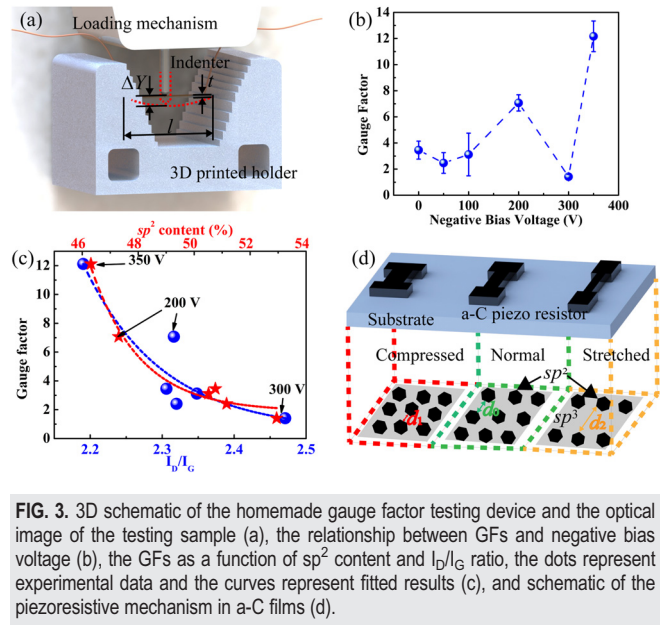


FIG. 3. 3D schematic of the homemade gauge factor testing device and the optical image of the testing sample (a), the relationship between GFs and negative bias voltage (b), the GFs as a function of sp^2 content and I_D/I_G ratio, the dots represent experimental data and the curves represent fitted results (c), and schematic of the piezoresistive mechanism in a-C films (d).

maximum GF was 12.1, corresponding to the minimum sp^2 content and the I_D/I_G ratio in the films. Considering that the deposited a-C films were hydrogen-free and dominated by graphitization, the change in electrical resistivity under force was the combined consequence of the sp^2 content and sp^2 cluster size. As shown in Fig. 3(c), interestingly, with an increase in the sp^2 content and I_D/I_G , the GFs nearly exponentially decreased in both cases, displaying the same behavior of GFs in response to changes in film graphitization and the sp^2 cluster size.

In the gauge factor testing experiment, compressive stress was applied to the sample during a force loading process, and thereafter, the electrical resistance of a-C films decreased, resulting from a tunneling effect of separated sp^2 clusters. The application of tensile stress caused the opposite result (supplementary material SIII). These results indicated that the correlation between GF, the sp^2 content, and L_a was consistent with the theory of thick film resistors.^{15,21} For this purpose, the a-C film can be described as a composite of conductive sp^2 clusters embedded in an insulating sp^3 matrix, and its resistivity is mainly controlled by carrier hopping between neighboring sp^2 clusters and will change with applied force or strain, since transport of the carriers between sp^2 clusters is realized by tunneling under force processing, as shown in Fig. 3(d). When force is applied to a-C piezoresistors, the distances between the conductive sp^2 clusters change [d_1 , d_2 in Fig. 3(d)], and as a result, a change in resistance is obtained. In the presented result, the sample with a higher sp^2 content and a larger sp^2 cluster size leads to a smaller initial distance, d_0 , between two adjacent sp^2 clusters. As a result, the same value of strain, ϵ , results in a smaller change in the distance, Δd , with $\Delta d = d_0\epsilon$. In other words, a decrease in the sp^2 content and the sp^2 cluster size causes a large increase in the GFs.

To further clarify the piezoresistive behavior of the integrated sensor, we chose the a-C sensor deposited at -200 V to fabricate the MEMS force sensor. Unlike other traditional tested resistance signals of a-C sensors,^{8,12,16,22,23} the voltage signals of the a-C based

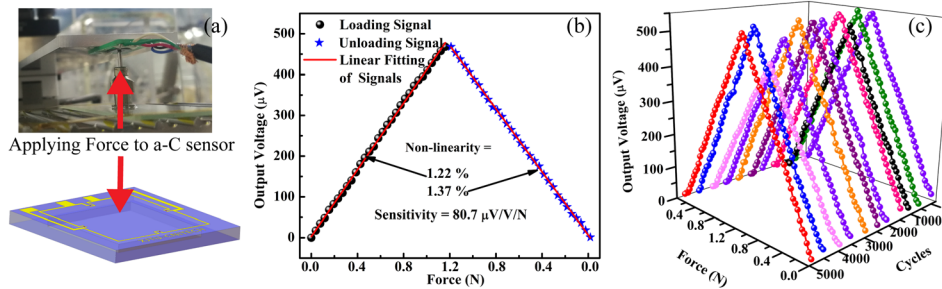


FIG. 4. Testing method for the a-C force sensor (a), the single cycle output signals of sensor's Wheatstone full-bridge (b), and 5000 cycles' testing result demonstrating sensor repeatability (c).

piezoresistive sensor which were collected in this work are much more common, easily recorded, and processed in the production control system. Figure 4(a) shows the testing method for the a-C force sensor. The force was applied by a flat pinhead, and its value was recorded using an electronic balance. A Wheatstone full-bridge consisting of four piezoresistors was used to convert strain into a voltage signal.²⁴ During a single loading and unloading cycle, as shown in Fig. 4(b), the force sensor showed a high sensitivity of $80.7 \mu\text{V/V/N}$, and the nonlinearities of the loading and unloading curves were 1.22% full scale (FS) and 1.37% FS, respectively. Moreover, the force sensor exhibited good repeatability after 5000 cycles [Fig. 4(c)] (the comparison with former works can be found in supplementary material SIII).

In conclusion, a higher sp^2 content and a larger size of the sp^2 cluster led to a lower GF for the a-C film. The correlation of piezoresistive behavior with atomic carbon bonds agreed well with the theory of thick film resistors. More importantly, a-C based MEMS force sensors were fabricated, and their performances were evaluated by voltage output signals. The force sensor showed a high sensitivity of $80.7 \mu\text{V/V/N}$, good linearity, and repeatability in 5000 test cycles, which demonstrated the promising application prospect of a-C films in MEMS sensors.

See the supplementary material for (SI) the deposition conditions and thickness of the a-C films and the adhesion test, (SII) the sp^2 content, fitted G-peak position, I_D/I_G , and FWHM of the G-peak in the a-C films and the ICP dry etching process, and (SIII) the comparison with former works and the typical $\Delta R/R$ -strain curve in gauge factor testing.

This research was supported by the National Natural Science Foundation of China (Nos. U1505244, 51805425, and 51602319), the Fundamental Research Funds for Central Universities (Nos. xzy022019038, and xjj2018046), Ningbo Science and Technology Innovation Project (No. 2018B10014), the Natural Science Foundation of Shaanxi Province (No. 2018JQ5018), and the Natural Science Foundation of Ningbo (No. 2018A610080).

REFERENCES

¹A. D. Smith, F. Niklaus, A. Paussa, S. Schroder, A. C. Fischer, M. Sterner, S. Wagner, S. Vaziri, F. Forsberg, D. Esseni, M. Ostling, and M. C. Lemme, *ACS Nano* **10**(11), 9879 (2016).

- ²H. R. Khalid, I. W. Nam, I. Choudhry, L. Zheng, and H. K. Lee, *Compos. Struct.* **203**, 835 (2018).
- ³K. Winkler, E. Bertagnolli, and A. Lugstein, *Nano Lett.* **15**(3), 1780 (2015).
- ⁴J. Robertson, *Mater. Sci. Eng., R* **37**(4–6), 129 (2002).
- ⁵K. Bewilogua and D. Hofmann, *Surf. Coat. Technol.* **242**, 214 (2014).
- ⁶S. Bhattacharyya and S. R. P. Silva, *Thin Solid Films* **482**(1–2), 94 (2005).
- ⁷P. Guo, R. Chen, L. Sun, X. Li, P. Ke, Q. Xue, and A. Wang, *Appl. Phys. Lett.* **112**(3), 033502 (2018).
- ⁸E. Peiner, A. Tibrewala, R. Bandorf, S. Biehl, H. Lüthje, and L. Doering, *Sens. Actuators, A* **130–131**, 75 (2006).
- ⁹A. Tibrewala, E. Peiner, R. Bandorf, S. Biehl, and H. Lüthje, *Appl. Surf. Sci.* **252**(15), 5387 (2006).
- ¹⁰A. Tibrewala, E. Peiner, R. Bandorf, S. Biehl, and H. Lüthje, *Thin Solid Films* **515**(20–21), 8028 (2007).
- ¹¹S. N. Meskinis, R. Gudaitis, K. Šlapikas, A. Vasiliasukas, A. Ciegis, T. Tamulevicius, M. Andrulevicius, and S. Tamulevicius, *ACS Appl. Mater. Interfaces* **10**(18), 15778 (2018).
- ¹²E. Peiner, A. Tibrewala, R. Bandorf, H. Lüthje, L. Doering, and W. Limmer, *J. Micromech. Microeng.* **17**(7), S83 (2007).
- ¹³A. Tibrewala, E. Peiner, R. Bandorf, S. Biehl, and H. Lüthje, *J. Micromech. Microeng.* **16**(6), S75 (2006).
- ¹⁴R. Kometani, K. Yusa, S. I. Warisawa, and S. Ishihara, *J. Vac. Sci. Technol., B* **28**(6), C6F38 (2010).
- ¹⁵S. Meskinis, A. Vasiliasukas, K. Šlapikas, R. Gudaitis, S. Tamulevicius, and G. Niaura, *Surf. Coat. Technol.* **211**, 172 (2012).
- ¹⁶B. Wang, Y. C. Jiang, R. Zhao, G. Z. Liu, A. P. He, and J. Gao, *J. Phys. D: Appl. Phys.* **51**(17), 175304 (2018).
- ¹⁷M. Jelínek, P. Písařík, T. Kocourek, J. Zemek, and J. Lukeš, *Appl. Phys. A* **110**(4), 943 (2013).
- ¹⁸A. C. Ferrari and J. Robertson, *Phys. Rev. B* **61**(20), 14095 (2000).
- ¹⁹M. Varga, T. Izak, V. Vretenar, H. Kozak, J. Holovsky, A. Artemenko, M. Hulman, V. Skakalova, D. S. Lee, and A. Kromka, *Carbon* **111**, 54 (2017).
- ²⁰Y. L. He, X. H. Wu, H. Y. Lin, H. Wang, and C. Li, *Chin. Sci. Bull.* **40**(20), 1684 (1995).
- ²¹C. Grimaldi, P. Ryser, and S. Strässler, *J. Appl. Phys.* **90**(1), 322 (2001).
- ²²S. Biehl, H. Lüthje, R. Bandorf, and J.-H. Sick, *Thin Solid Films* **515**(3), 1171 (2006).
- ²³S. Uhlig, H. Schmid-Engel, T. Speicher, and G. Schultes, *Sens. Actuators, A* **193**, 129 (2013).
- ²⁴E. Peiner, A. Tibrewala, R. Bandorf, S. Biehl, H. Lüthje, and L. Doering, in *Proceedings of the International Conference on Smart Systems Integration 2007, Paris, France, 27–28 March 2007*, edited by T. Gessner (VDE-Verlag, Berlin, 2007), pp. 257–264.